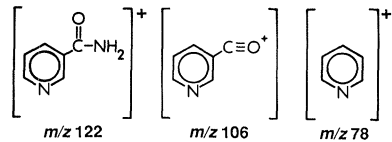


12. The corneal micropocket assay was performed in rabbits by G. Luty and R. Mello, of Johns Hopkins University School of Medicine, by methods similar to those described by G. A. Fournier, G. A. Luty, S. Watt, A. Fenselau, and A. Patz [*Invest. Ophthalmol. Visual Sci.* **21**, 351 (1981)].
13. Methanol solutions of P2, P3, or commercial nicotinamide were analyzed with a Nermag R 10-10 quadrupole mass spectrometer; a 60- $\mu$ m tungsten wire was used for the desorption surface. The three largest ions observed, mass-to-charge ratio ( $m/z$ ) 122, 106, and 78, are suggested in the diagram below. For the methodology, see B. Soltmann, C. C. Sweeley, and J. F. Holland [*Anal. Chem.* **49**, 1164 (1977)] and D. F. Hunt, J. Shabanowitz, F. K. Botz, and D. A. Brent (*ibid.*, p. 1160).



14. The NMR spectrum data are as follows:  $\delta$  9.03 (1H, dd,  $J_{2,4} = 2.1$ ,  $J_{2,5} = 0.6$ , H2);  $\delta$  8.70 (1H, dd,  $J_{5,6} = 4.8$ ,  $J_{4,6} = 1.7$ , H6);  $\delta$  8.22 (1H, ddd,  $J_{4,5} = 7.9$ , H4); and  $\delta$  7.50 (1H, ddd, H5).
15. A Durabond DB-1 (J and W Scientific) capillary

column was programmed from 100° to 270°C at 10° per minute. Electron impact was the mode of ionization. The mass spectrometer was a Nermag R 10-10 quadrupole.

16. M. N. Ellis, unpublished results.
17. Elvax 40 "sandwich" pellets similar to those used in Fig. 1 were made, except that they incorporated 0.1  $\mu$ Ci of [*carbonyl*-<sup>14</sup>C]nicotinamide with and without potassium phosphate. Pellets were placed in 0.25 ml of Hanks buffer. The solution was replaced at 1, 2, 4, 8, 24, 48, 72, 96, 192, 288, and 384 hours. Release rates were related to the recovery of radioactivity. Fifteen percent of the nicotinamide was released in the first 48 hours as compared to 36% in the group of pellets containing the salt. The release rates were not significantly different over the next 12 days.
18. R. Langer and J. Folkman, *Nature (London)* **263**, 797 (1976); D. M. Form and R. Auerbach, *Proc. Soc. Exp. Biol. Med.* **172**, 214 (1983).
19. B. R. Clark *et al.*, *Cancer Res.* **35**, 1727 (1975).
20. D. Gospodarowicz *et al.*, *Proc. Natl. Acad. Sci. U.S.A.* **81**, 6963 (1984).
21. R. Nunez, E. Calva, M. Marsch, E. Briones, F. López-Soriano, *Am. J. Physiol.* **231**, 1173 (1976); H. H. Klein *et al.*, *Basic Res. Cardiol.* **76**, 612 (1981).
22. H. H. Klein, S. Puschmann, J. Schaper, W. Schaper, *Virchows Arch. A* **393**, 287 (1981); R. Klover, J.

- Darsec, L. De Boer, N. Carlson, *Arch. Pathol. Lab. Med.* **105**, 403 (1981).
23. G. T. Williams, C. C. Ford, S. Shall, *Biochem. Biophys. Res. Commun.* **108**, 36 (1982).
24. F. Farzanek and C. K. Pearson, *Dev. Biol.* **72**, 254 (1979).
25. P. Mandel, H. Okazaki, C. Niedergang, *Prog. Nucleic Acid Res. Mol. Biol.* **27**, 1 (1982).
26. G. Tornling *et al.*, *Cardiovasc. Res.* **12**, 692 (1978); T. Mattfeldt and G. Mall, *ibid.* **17**, 229 (1983).
27. G. Tassi and P. De Nicola, *Curr. Ther. Res. Clin. Exp.* **30**, 98 (1981).
28. W. Bethmann, H.-A. Gitt, I. Gitt, *Z. Exp. Chir.* **11**, 238 (1978).
29. B. Körlof and O. Ugland, *Acta Chir. Scand.* **131**, 408 (1966); J. Benfer and H. Struck, *Arzneim. Forsch.* **28**, 37 (1978).
30. T. Myczkowski, *Med. Klin.* **70**, 861 (1975).
31. We thank G. Luty and R. Mello for the angiogenic determinations; A. Fenselau for the Walker 256 carcinoma, preprints, and informative discussion; R. Bonser for interest and discussion; P. Bhattacharjee for confirmatory studies on the angiogenic activity of nicotinamide in the rabbit corneal micropocket assay; M. N. Ellis for studies with the chick chorioallantoic membrane assay; and C. Barry for information services.

24 September 1986; accepted 2 March 1987

## Efficient Packaging of Readthrough RNA in ALV: Implications for Oncogene Transduction

STEVEN A. HERMAN\* AND JOHN M. COFFIN

Readthrough viral transcripts are present at relatively high levels in cells infected with avian leukosis virus. It has been proposed that they can function as intermediates in the transduction of proto-oncogenes by retroviruses. It is shown here, by the analysis of viruses containing a mutation in the AAUAAA polyadenylation signal, that readthrough RNAs have the requisite properties to function as transduction intermediates: (i) readthrough RNAs were polyadenylated and packaged as efficiently as normal viral RNA, (ii) RNAs nearly 11.2 kilobases (3.5 kilobases larger than wild-type avian leukosis virus genomes) were present in virions of the mutant virus, and (iii) virus particles containing both readthrough and normal genomes were most likely infectious.

INTEGRATED PROVIRAL DNA OF RETROVIRUSES is flanked by long terminal repeats (LTRs) that contain transcriptional regulatory signals recognized by the host cell. Although identical in sequence, the LTRs are distinct in function. Viral transcription is initiated within the 5' (upstream) LTR; cleavage and polyadenylation of viral transcripts occur within RNA derived from the 3' (downstream) LTR. Transcripts initiated within the 3' LTR (downstream transcripts) are normally undetectable (1).

Integration of proviral DNA in the vicinity of cellular proto-oncogenes can cause malignant disease in the host, due to the effects of viral transcriptional signals on the expression of adjacent cellular genes. In avian leukosis virus (ALV)-induced erythroblastosis, the expression of the proto-oncogene *c-erbB* can be activated by readthrough transcripts, that is, viral RNAs that escape cleavage and polyadenylation at the normal

site and thus extend into the downstream *c-erbB* gene (2). In ALV-induced lymphoma, expression of the *c-myc* gene is usually activated by viral transcripts initiated within the 3' LTR, that is, downstream RNAs (3). In addition, new ALV-related viruses that contain oncogenes are occasionally recovered from animals with ALV-induced malignancies (4, 5).

Proviral integration within or adjoining a proto-oncogene is thought to be an essential step in the acquisition of oncogenes by retroviruses. A multistep model has been proposed for oncogene capture as follows (6): (i) integration of proviral DNA within or upstream of a proto-oncogene, in the same transcriptional orientation; (ii) deletion of the 3' proviral DNA to fuse the proto-oncogene to the viral transcriptional unit; (iii) transcription of the deleted provirus to produce an RNA containing both viral and proto-oncogene sequences; (iv) packaging of the chimeric transcripts and

normal viral genomes into virus particles; and (v) use of both molecules as templates during reverse transcription, that is, template switching (7), resulting in the formation of a new provirus containing the oncogene. Alternatively, oncogene transduction could be accomplished entirely at the RNA level, without a chromosomal deletion, by the generation and packaging into virions of readthrough transcripts that contain the proto-oncogene (8). This scheme requires (i) that readthrough transcripts be produced and efficiently packaged into infectious virus particles and (ii) that virus particles accommodate readthrough RNAs of adequate size. In previous work we found readthrough RNAs at high levels in infected cells, amounting to 15% of the total viral RNA (1). In this report we show efficient incorporation of readthrough RNAs into infectious virus. Furthermore, virions can accommodate RNAs nearly 11.2 kb in size, 3.5 kb longer than the genome RNA of ALV.

To characterize the biological effects of readthrough transcripts, we found it desirable to increase their abundance. Thus, we introduced a point mutation into the polyadenylation [poly(A)] signal of a DNA clone of Rous sarcoma virus (RSV) by means of oligonucleotide-directed mutagenesis (Fig. 1). Infectious virus was recovered after transfection of turkey embryo fibroblasts (TEF) with the mutant and wild-type DNAs, and was used to infect fresh TEF

Department of Molecular Biology and Microbiology, Tufts University School of Medicine, Boston, MA 02111.

\*Present address: Department of Cell Biology, Roche Institute of Molecular Biology, Nutley, NJ 07110.

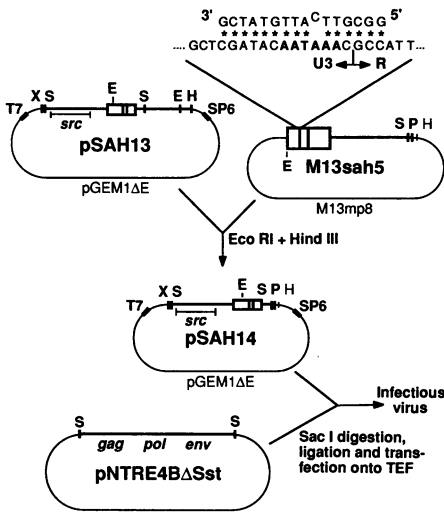


**Fig. 1.** Introduction of a point mutation into the polyadenylation signal of ALV. M13sah5 contained a 328-bp fragment from the Eco RI site (nucleotide -53 relative to the cap site of viral RNA) to the Pst I site (nucleotide 263) from pATV-8, a molecular clone of the Prague C strain of RSV (17), inserted into M13mp8 (18). A 16-base oligonucleotide was used to alter the polyadenylation signal to AAUGAA, according to the method of Kunkel (19). The plasmid pSAH13 contained a 5.2-kb fragment from the Xba I site (nucleotide 6861) to the Hind III site (nucleotide 2740) from pATV-8 inserted into pGEM1ΔE [pGEM1 (20), lacking the Eco RI site in the polycloning site]. The LTR-containing Eco RI to Hind III fragment from several clones of M13sah5 that had acquired the point mutation

and from two wild-type clones were ligated individually to the large Eco RI to Hind III fragment from pSAH13 to create the pSAH14 series of plasmids, which contained the *src* gene, LTR, and 5' viral sequences on a 2.7-kb Sac I fragment. The remainder of the viral sequences were present on plasmid pNTRE4BΔSst, on a 6.6-kb Sac I fragment (21). The pSAH14 plasmids were digested with Sac I and ligated individually to Sac I-digested pNTRE4BΔSst. Infectious transforming virus was recovered from the mutant and wild-type constructions by transfection of the ligated DNAs onto TEF, by the *O*-diethylaminoethyl (DEAE)-dextran method (14). Filled boxes indicate bacteriophage SP6 and T7 promoters. Abbreviations: X, Xba I; S, Sac I; E, Eco RI; H, Hind III; P, Pst I. Not to scale.

from which cellular and virion RNAs were isolated.

Viral RNAs polyadenylated at the normal site can be distinguished from readthrough RNAs by protection from nuclease digestion of a uniformly labeled probe complementary to the viral U3-R-U5-leader

sequence (Fig. 2B) (1). Analysis of total RNA from TEF infected with wild-type (W10.18) or mutant (M9.13) viruses revealed the presence of both correctly processed and readthrough viral RNAs (Fig. 2A). In agreement with our prior results, downstream RNA was not detected (1). Comparison of the relative intensities of the 3' RNA bands, corresponding to viral RNA cleaved at the normal poly(A) site, and the

readthrough RNA bands shows that most of the viral RNA was correctly processed in cells infected with the wild-type virus (Fig. 2A, lanes 5 to 8). However, in cells infected with the mutant virus, most of the viral RNA was readthrough RNA (Fig. 2A, lanes 9 to 12). The relative numbers of probe molecules in each band were calculated from their radioactivity (9). Taking the sum of the probe molecules in the 3' RNA and readthrough RNA bands as a measure of the total viral RNA, readthrough RNA amounted to 16% of the viral RNA in cells infected with the wild-type virus and 80% of

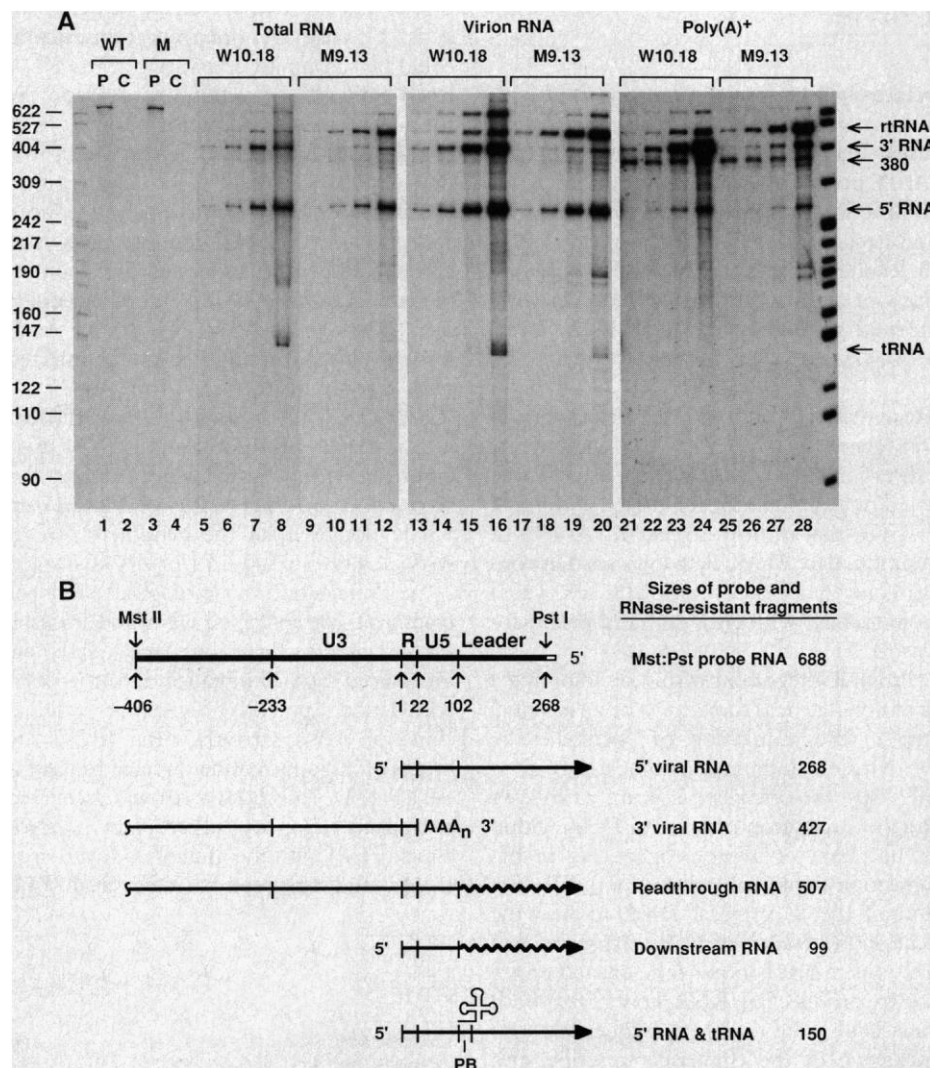


**Fig. 2.** Nuclease protection analysis of virion and cellular RNA. (A) <sup>32</sup>P-labeled wild-type (WT) or mutant (M) probe RNAs were hybridized to total cellular RNA, virion RNA, or poly(A)<sup>+</sup> cellular RNA from TEF infected with the wild-type (W10.18) or the mutant (M9.13) viruses, treated with RNase, and subjected to polyacrylamide gel electrophoresis. Hybridizations were performed with 0.1-pmol of probe RNA and 0.3, 1.0, 3.0, and 10.0 μg of total RNA (lanes 5 to 8 and 9 to 12, respectively), virion RNA isolated from 40, 120, 400, and 1200 μl of culture supernatants (lanes 13 to 16 and 17 to 20, respectively), poly(A)<sup>+</sup> RNA isolated from 0.6, 2.0, 6.0, and 20.0 μg of total RNA from infected TEF (lanes 21 to 24 and 25 to 28, respectively), and 20 μg of carrier yeast RNA (C, lanes 2 and 4). The probes were synthesized with SP6 RNA polymerase using as templates the plasmids pSAH14-M9.13 or pSAH14-W10.18 digested with Mst II (Fig. 1). Lanes 1 and 3 contained 0.001 pmol of undigested probe RNA (P). Similar probes did not hybridize to RNA from uninfected TEF. Isolation of cellular RNA, synthesis of probe RNA, and nuclease protection analysis were performed as described (1). A band of 380 nucleotides present in all the lanes (except lanes 1 and 3) is an artifactual band derived from the template used for probe synthesis. It is more apparent in lanes 21 to 28, for which a longer exposure is shown. The band of about 140 nucleotides results from competition between the probe RNA and the transfer RNA (tRNA) primer (22); rRNA, readthrough RNA. (B) Structure of probe RNA and sizes of RNase-resistant probe fragments protected by viral RNAs. Solid bar, probe RNA complementary to viral RNA; open bar, nonviral sequence at the 5' end of the probe; wavy lines, cellular sequences in readthrough and downstream RNAs; PB, primer binding site.

the viral RNA in cells infected with virus M9.13. However, the mutation did not greatly affect the overall level of viral RNA production. Comparison of the radioactivity in the 5' RNA bands, corresponding to both normal and readthrough RNAs, showed that the level of viral RNA in cells infected with virus M9.13 was about 55 to 75% of that in cells infected with virus W10.18. Analysis with probes of different sizes and of independently isolated clones of the mutant and wild-type viruses yielded the same results. In addition, the phenotype and structure of the mutant viruses were confirmed by direct analysis of virion RNA by ribonuclease (RNase) T1 oligonucleotide fingerprinting (10).

In previous work we showed that readthrough RNA in ALV-infected cells is polyadenylated to the same extent as normal viral RNA (1). Analysis of poly(A)<sup>+</sup> RNA from TEF infected with viruses W10.18 or M9.13 confirmed this observation for the mutant virus as well (Fig. 2A). The ratios of the intensities of the readthrough RNA bands to the 3' RNA bands in the poly(A)<sup>+</sup> RNA samples were very similar to the ratios in the corresponding total RNA samples, which indicated that readthrough RNA was polyadenylated as efficiently as normal viral RNA (11).

These results demonstrated that the mutation in the AAUAAA polyadenylation signal caused the predicted phenotype. Viral RNA was synthesized and processed at nearly wild-type levels. However, the large majority was polyadenylated not at the usual site but at alternative sites most likely derived from the cellular DNA downstream of the integration site.

Nuclease protection analysis of virion RNA indicated that readthrough RNA was packaged into virions as efficiently as normally processed viral RNA. Readthrough RNA amounted to about the same fraction of the total viral RNA in virions as it did in infected cells, for virus M9.13 and virus W10.18 (Fig. 2A). Measurement of the radioactivity in individual bands (9) showed that readthrough transcripts amounted to 20% of viral RNA in wild-type virus particles and 86% of viral RNA in mutant virions. This finding suggests, surprisingly, that if normal and readthrough RNAs were distributed randomly in virions, then 32% of the wild-type virus particles may have contained both normal and readthrough RNAs (12).

The size distribution of readthrough transcripts was examined by subjecting virion RNA and poly(A)<sup>+</sup> RNA from infected cells to gel electrophoresis and hybridization analysis with a probe complementary to the virus leader region (Fig. 3). Poly(A)<sup>+</sup> RNA

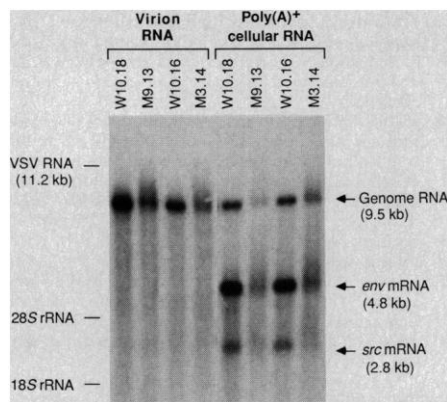


**Fig. 3.** Size fractionation of cellular and virion RNA. Virion RNA isolated from 400  $\mu$ l of culture supernatant and poly(A)<sup>+</sup> RNA isolated from 20  $\mu$ g total RNA from TEF infected with the indicated viruses were subjected to electrophoresis through a 0.4% agarose gel containing formaldehyde (23). The RNA was transferred to a nylon membrane and hybridized to a uniformly labeled RNA probe complementary to the viral leader region from the BstE II site (nucleotide 103) to the Sac I site (nucleotide 255); VSV, vesicular stomatitis virus.

from infected cells contained three viral species corresponding to genome RNA, *env* messenger RNA (mRNA), and *src* mRNA. However, the viral RNA species from cells infected with the mutant viruses were indistinct. The lower size limit for each species was discrete and the same as that for the corresponding species derived from the wild-type viruses, but the upper size limit was indistinct, with the intensity of the band decreasing with increasing molecular weight. Thus, the polyadenylation mutation decreased the efficiency of 3' processing at the normal viral site, leading to the production of longer transcripts, which were polyadenylated at downstream sites. Both full-length genome RNA and spliced subgenomic mRNAs were affected by the mutation. The effect of the mutation on the size distribution of viral RNAs is more obvious for *src* mRNA because of the increased resolution of smaller RNAs on the gel.

Analysis of virion RNA showed that RNAs nearly 11.2 kb in size were packaged into the mutant virions (Fig. 3). The largest genome sizes reported for infectious avian retroviruses are about 10.2 kb (13, 14). Wild-type virions contained RNAs larger than genome length as well, but to a smaller degree.

Virus replication was reduced slightly by the poly(A) mutation. The titers of the mutant viruses were three to six times less than those of the wild-type viruses (15). This difference cannot be due solely to the lower level of viral RNA production from the mutant viruses, which differed from the wild type by less than a factor of 2 (Fig. 2A).

The result suggests that virus particles containing both readthrough RNA and normal genomes were infectious, but that those containing only readthrough RNAs were not. If readthrough RNAs and normally processed genomes were distributed randomly in virus particles, then 64% of wild-type virions but only 2% of mutant virions would contain two normal genomes (12). Thus, if two normal genomes were required for infectivity, then the titers of the mutant viruses would have been at least 30-fold less than those of the wild-type viruses.

To determine if the mutant virus stocks contained revertants that could account for the residual level of correct 3' processing, we analyzed the RNA of six clones of the mutant viruses, isolated by focus formation in soft agar. In five of the six clones readthrough RNA amounted to about 80% of the total viral RNA; one clone was a revertant. Furthermore, the level of readthrough RNA remained the same after repeated cycles of infection and growth of the mutant virus. Thus, the residual correct processing was not due to revertants, and, although one revertant was found, revertants did not occur and grow with sufficient frequency and speed to affect the phenotype of the population.

Our prior observation that readthrough RNA is present at relatively high levels in ALV-infected cells suggested that readthrough transcripts could function as intermediates in the transduction of oncogenes, as has been suggested (8). We show here that readthrough transcripts have the properties required of transduction intermediates: they are efficiently processed and packaged into infectious virus particles. Thus both recombination events needed for oncogene transduction could occur at the RNA level: the 3' recombination by template switching during reverse transcription (7) and the 5' crossover by splicing or during reverse transcription (6). There is considerable indirect evidence for illegitimate recombination during reverse transcription (8, 16), and the transductions of *c-erbB* frequently observed in avian erythroblastosis are most likely examples of oncogene capture by this mechanism (2, 5).

#### REFERENCES AND NOTES

1. S. A. Herman and J. M. Coffin, *J. Virol.* **60**, 497 (1986).
2. T. W. Nilsen *et al.*, *Cell* **41**, 719 (1985).
3. B. G. Neel, W. S. Hayward, H. L. Robinson, J. Fang, S. M. Astrin, *ibid.* **23**, 323 (1981); W. S. Hayward, B. G. Neel, S. M. Astrin, *Nature (London)* **290**, 475 (1981); G. S. Payne *et al.*, *Cell* **23**, 311 (1981); Y.-K. T. Fung, A. M. Fady, L. B. Crittenden, H.-J. Kung, *Proc. Natl. Acad. Sci. U.S.A.* **78**, 3418 (1981); G. S. Payne, J. M. Bishop, H. E. Varmus, *Nature (London)* **295**, 209 (1982); H. L. Robinson and G. C. Gagnon, *J. Virol.* **57**, 28 (1986).
4. J. M. Bishop and H. Varmus, in *RNA Tumor*

- Viruses, Molecular Biology of Tumor Viruses*, R. Weiss, N. Teich, H. Varmus, J. Coffin, Eds. (Cold Spring Harbor Laboratory, Cold Spring Harbor, NY, ed. 2, 1985), pp. 249–356.
5. B. D. Miles and H. L. Robinson, *J. Virol.* **54**, 295 (1985).
  6. S. P. Goff, E. Gilboa, O. N. Witte, D. Baltimore, *Cell* **22**, 777 (1980); H. E. Varmus, *Science* **216**, 812 (1982); R. Swanstrom, R. C. Parker, H. E. Varmus, J. M. Bishop, *Proc. Natl. Acad. Sci. U.S.A.* **80**, 2519 (1983); J. M. Bishop, *Annu. Rev. Biochem.* **52**, 301 (1983).
  7. J. M. Coffin, *J. Gen. Virol.* **42**, 1 (1979).
  8. M. P. Goldfarb and R. A. Weinberg, *J. Virol.* **38**, 136 (1981).
  9. The bands were excised and the <sup>32</sup>P was measured by liquid scintillation counting. The background radioactivity was determined separately for each band from a gel fragment immediately above each band. The relative numbers of probe molecules in each band of a given lane were then calculated by correcting the counts per minute in each band for the number of labeled bases in the corresponding probe fragment.
  10. K. F. Conklin *et al.*, *Mol. Cell. Biol.* **2**, 638 (1982).
  11. The 5' RNA bands were diminished in the poly(A)<sup>+</sup> samples, relative to the other bands, since the 5' sequences were further from the poly(A) tract and thus recovered during poly(A) selection at lower efficiency.
  12. If we assume random distribution of read-through and normal RNAs in virions, then the composition of genome dimer complexes would be as follows: for wild-type virions, 64% normal-normal, 32% readthrough-normal, and 4% readthrough-readthrough; for mutant virions, 2% normal-normal, 24% readthrough-normal, and 74% readthrough-readthrough.
  13. J. Sorge and S. H. Hughes, in *Eucaryotic Viral Vectors*, Y. Gluzman, Ed. (Cold Spring Harbor Laboratory, Cold Spring Harbor, NY, 1982), pp. 127–132; D. A. Foster and H. Hanafusa, *J. Virol.* **48**, 744 (1983).
  14. P. A. Norton and J. M. Coffin, *Mol. Cell. Biol.* **5**, 281 (1985).
  15. The concentrations of focus-forming units (FFU) were measured in the same culture supernatants from which virion RNA was isolated. The titers were  $1.6 \times 10^7$  FFU/ml and  $2.4 \times 10^7$  FFU/ml for M3.14 and M9.13, and  $7.3 \times 10^7$  FFU/ml and  $8.9 \times 10^7$  FFU/ml for W10.16 and W10.18, respectively.
  16. C.-C. Huang, N. Hay, J. M. Bishop, *Cell* **44**, 935 (1986).
  17. R. A. Katz *et al.*, *J. Virol.* **42**, 346 (1982).
  18. J. Messing, *Methods Enzymol.* **101**, 20 (1985).
  19. T. A. Kunkel, *Proc. Natl. Acad. Sci. U.S.A.* **82**, 488 (1985).
  20. Promega Biotech.
  21. A. J. Dorner, J. P. Stoye, J. M. Coffin, *J. Virol.* **53**, 32 (1985).
  22. S. A. Herman, thesis, Tufts University, Medford, MA (1986).
  23. T. Maniatis, E. F. Fritsch, J. Sambrook, *Molecular Cloning: A Laboratory Manual* (Cold Spring Harbor Laboratory, Cold Spring Harbor, NY, 1982), p. 199.
  24. We thank T. Henkin and P. Hopper for advice on site-directed mutagenesis and high-performance liquid chromatography. This work was supported by Public Health Service grant CA17659 from the National Cancer Institute.

17 November 1986; accepted 25 February 1987

## Formation of Retinal Ganglion Cell Topography During Prenatal Development

BARRY LIA, ROBERT W. WILLIAMS,\* LEO M. CHALUPA

A fundamental feature of the mammalian visual system is the nonuniform distribution of ganglion cells across the retinal surface. To understand the ontogenetic processes leading to the formation of retinal ganglion cell topography, changes in the regional density of these neurons were studied in relation to ganglion cell loss and the pattern of retinal growth in the fetal cat. Midway through the gestation period, the density of these neurons was only two to three times greater in the area centralis than in the peripheral retina, whereas shortly before birth this central-to-peripheral difference was nearly 20-fold. Age-related changes in the ganglion cell distribution were found not to correspond in time or magnitude to the massive loss of ganglion cells that occurs during prenatal development. Rather, the formation of ganglion cell density gradients can be accounted for by unequal expansion of the growing fetal retina—peripheral regions expand more than the central region, thereby diluting the peripheral density of ganglion cells to a greater degree. Nonuniform growth, in conjunction with differential periods of neurogenesis of the different types of retinal cells, appears to be a dominant factor regulating overall retinal topography. These results suggest that the differential regional expansion of the fetal retina underlies the formation of magnification factors in the developing visual system.

**I**N ANIMALS WITH HIGHLY DEVELOPED focal vision the distribution of ganglion cells across the retinal surface is strikingly nonuniform. The density of ganglion cells peaks around the fovea or area centralis—the region of the retina specialized for focal vision—and declines sharply toward the periphery (1). This central-to-peripheral gradient in ganglion cell topography dominates retinotopic maps in the visual centers of the brain and is related to variations in measures of acuity across the visual field (2).

The development of ganglion cell density gradients poses an intriguing problem because regional specialization in the ganglion cell layer is reflected in the neuronal circuitry throughout the visual system. Early in development the regional distribution of ganglion cells is relatively uniform (3–5), and the number of these neurons is much greater in

the fetal retina than at maturity (6, 7). It has been proposed that differential ganglion cell death across the retina is responsible for the establishment of ganglion cell topography (3, 8). This would be the case if during ontogeny greater numbers of ganglion cells die in the peripheral retina than in the central retina. A substantial amount of cell death does occur during development of the mammalian retina. For instance, it has been estimated that in the cat five of six ganglion cells generated during fetal life are eliminated by maturity (6). However, it remains to be determined whether such massive loss of neurons contributes significantly to the formation of retinal topography.

An alternative explanation for the establishment of ganglion cell topography is the nonuniform expansion of the growing retina. During ontogeny the growth of the

peripheral retina could be greater than that of the central retina, thereby diluting the peripheral population of ganglion cells to a greater degree. Such a pattern of retinal growth has been shown to occur in the postnatal cat (9), and this process may also be a key factor in sculpting the distribution pattern of retinal ganglion cells during fetal development.

In this study, we describe developmental changes in the distribution of ganglion cells across the retina of prenatal cats and relate these findings to ganglion cell loss and retinal growth. We show that a primordial area centralis is present early in development and that the progressive increase in the central-to-peripheral gradient in ganglion cell density results primarily from differential expansion of the retina rather than ganglion cell loss.

Ganglion cell topography was examined in fetal cats ranging in age from day 35 of gestation (E35)—just after ganglion cell generation has ended (10) and after the initial innervation of retinorecipient nuclei (11, 12)—to E62, about 3 days before birth. All surgical procedures were carried out under aseptic conditions with the use of 1 to 2% halothane in oxygen supplemented with 30% nitrous oxide. To identify centrally projecting retinal ganglion cells, 2 to 15  $\mu$ l of horseradish peroxidase or horseradish peroxidase conjugated to wheat germ agglutinin was injected bilaterally into the posterior thalamus and midbrain or into the optic chiasm. This retrograde labeling procedure was necessary because it is not possible to unequivocally differentiate ganglion cells from other cell types in the ganglion cell

Department of Psychology and the Physiology Graduate Group, University of California, Davis, CA 95616.

\*Present address: Section of Neuroanatomy, Yale University School of Medicine, New Haven, CT 06510.